



Prostate cancer evaluation using PET quantification in ^{68}Ga -PSMA-11 PET/MR with attenuation correction of bones as a fifth compartment

Liran Domachevsky^{1,2}, Natalia Goldberg¹, Miguel Gorenberg³, Hanna Bernstine^{1,2}, David Groshar^{1,2}, Onofrio A. Catalano⁴

¹Department of Nuclear Medicine, Assuta Medical Centers, Tel Aviv 6971028, Israel; ²Sackler School of Medicine, Tel Aviv University, Tel Aviv 6997801, Israel; ³Department of Nuclear Medicine, Bnai Zion Medical Center and Faculty of Medicine, The Technion-Israel Institute of Technology, Haifa 3339419, Israel; ⁴Athinoula A. Martinos Center for Biomedical Imaging, Department of Radiology, Massachusetts General Hospital, Harvard Medical School, Charlestown, MA, USA

Correspondence to: Prof. David Groshar, MD. Department of Nuclear Medicine, Assuta Medical Center, 20 Habarzel Street, Tel Aviv 6971028, Israel. Email: davidg@assuta.co.il.

Background: Tissues with low magnetic resonance (MR) signals, such as bones and lungs differ considerably in their attenuation properties, requiring special considerations for attenuation correction. We evaluated the impact of using the five-compartment segmentation model, which incorporates bones, in ^{68}Ga -PSMA-11 PET/MR studies in patients undergoing evaluation for prostate cancer.

Methods: Prostate cancer patients underwent dedicated prostate ^{68}Ga -PSMA-11 PET/MR followed by whole-body ^{68}Ga -PSMA-11 PET/CT. Coronal μmap images of the pelvis derived from four- and five-compartment segmentation models of magnetic resonance attenuation correction (MRAC) were produced. Standardized uptake values (SUV) calculated by the four and five-compartment MRAC models and by computed tomography attenuation correction (CTAC) were compared and correlated in normal prostate tissue, gluteus muscle, sacrum, intra-prostatic lesions and metastases (i.e., bone lesions and involved lymph nodes), and prostatic lesions to gluteus (L/G) ratio.

Results: Twenty-six patients (mean age 69.4 ± 9.3 years) were included in the study. Twenty-five patients presented for prostate cancer staging and one patient was evaluated for recurrent disease. There was a statistically significant difference between SUVs of the gluteus, sacrum, prostatic lesions and normal prostate tissue measured by the four-compartment *vs.* the five-compartment MRAC models, with a medium effect size. Very good to good correlation between SUV measured using the four-compartment MRAC model and SUV measured using the five-compartment model were noted in all lesional and non-lesional areas. Very good to good correlation was noted between four-compartment MRAC and CTAC SUVs of prostatic lesions and L/G ratio and between five-compartment MRAC and CTAC SUVs of prostatic lesions, L/G ratio and metastatic lesions.

Conclusions: ^{68}Ga -PSMA-11 PET/MR using the five-compartment segmentation model affects SUV measurements in prostate lesions and in the normal prostate and therefore patient follow-up studies must be conducted using the same segmentation model.

Keywords: Bones; positron emission tomography computed tomography (PET CT); prostatic neoplasms

Submitted Jul 28, 2019. Accepted for publication Nov 19, 2019.

doi: 10.21037/qims.2019.11.19

View this article at: <http://dx.doi.org/10.21037/qims.2019.11.19>

Introduction

Unlike positron emission tomography (PET)-computed tomography attenuation correction (CTAC) of images, whereby Hounsfield units are converted to linear attenuation coefficients, PET-magnetic resonance attenuation correction (MRAC) of images relies on proton density and tissue relaxation times that cannot be easily “translated” to linear attenuation coefficients. Moreover, tissues with low MR signals, such as bones and lungs, necessitate special consideration as both produce similar MR images but differ considerably in their attenuation properties. As a result, segmentation models have been applied whereby the body is divided into four major compartments—fat, air, lung and soft tissue—each of which is assigned a fixed linear attenuation correction (AC) number (1). However, several studies have shown that MRAC using the four-compartment segmentation model results in underestimation of standardized uptake values (SUVs) compared to CTAC, particularly in the presence of bone lesions or lesions that are adjacent to bones (2). As attenuation coefficients of soft tissues are often applied to bones, a five-compartment segmentation model that includes the bones has been introduced recently. This model has yielded improved accuracy of MRAC in studies using the radiotracers ^{18}F -fluorodeoxyglucose (^{18}F -FDG) and ^{18}F -Fluciclovine (3,4).

^{68}Ga -gallium-labeled prostate-specific membrane antigen 11 (^{68}Ga -PSMA-11) PET/MR is an emerging modality that combines, in one procedure, information on PET-derived PSMA receptor expression in prostate tumours and MR-derived anatomical and functional information. In contrast to the sequential acquisition of PET and CT images for PET/CT studies, which necessitates good registration between the images in order to obtain good image quality and accurate SUV measurements, in PET/MR studies the MR and PET images are acquired simultaneously, resulting in theoretically ideal image co-registration. Several studies have shown the added diagnostic value of ^{68}Ga -PSMA-11 PET/MR, over multi-parametric MRI, for detection (5), localization (6) and characterization (7,8) of tumours and involved lymph nodes (5) in patients undergoing initial evaluation for prostate cancer. ^{68}Ga -PSMA-11 PET/MR has also been shown to be accurate and reliable, compared to ^{68}Ga -PSMA-11 PET/CT, in depicting nodal and osseous metastases (9,10) and in the pre-operative prediction of T and N stages in high-risk prostate cancer patients (11).

Limited pelvic ^{68}Ga -PSMA-11 PET/MR has also been shown to be useful for the initial evaluation of histological biopsy-proven prostate cancer and to be superior to PET/CT in detecting extensions of localized disease, mainly due to the high soft tissue resolution of MR (12).

We evaluated the five-compartment segmentation model, which incorporates bones, in ^{68}Ga -PSMA-11 PET/MR studies in patients undergoing evaluation for prostate cancer.

Methods

Patients and setting

This retrospective study of prospectively collected data was approved by the institutional ethics committee (approval number, 2015024). Between December 2017 and February 2018, 26 consecutive prostate cancer patients scheduled for a clinically-indicated ^{68}Ga -PSMA PET/CT study—either for initial staging of prostate cancer or due to biochemical recurrence after therapy—were contacted by the study coordinator and offered to participate in the study. Written informed consent was obtained from all patients prior to study participation.

^{68}Ga -PSMA-11 PET/MR protocol

The patients underwent a dedicated ^{68}Ga -PSMA-11 PET/MR of the prostate immediately after receiving a tracer injection dose of 2–4 mCi (75–150 MBq). The patients were instructed to urinate before the study and none of them underwent urethral catheterization.

^{68}Ga -PSMA-11 PET/MR was performed on the Biograph mMR (Siemens AG, Healthcare Sector, Erlangen, Germany) using the syngo MR E11P operational system. The patients were placed in the supine position and only their pelvis was covered with a 24-channel spine radiofrequency (RF) coil integrated within the MR bed and a surface body coil (each of them comprising 6 channels). PET scanning of the pelvis began immediately after ^{68}Ga -PSMA-11 administration with an acquisition time of 20 minutes. PET data were acquired in the list mode with the following reconstruction parameters: high definition PET + ordered subset expectation maximization (OSEM) iterative algorithm, 3 iterations and 21 subsets, Gaussian filter: full width at half maximum (FWHM) 4.0 mm; scattered correction.

Table 1 Early ⁶⁸Ga-PSMA PET/MR sequences and PET acquisition time

Early ⁶⁸ Ga-PSMA PET/MR sequences	PET acquisition time
Prostate 3D TSE sequence (SPACE)	20 minutes
MRAC PET	
Pre contrast T1 VIBE	
Dynamic T1 VIBE	
Late T1 VIBE	
Diffusion-weighted imaging	
Prostate T2 HASTE sagittal + coronal + transverse	

HASTE, half-Fourier acquired single turbo spin-echo; IR, inversion recovery; PET MRAC, positron emission tomography-magnetic resonance attenuation correction; SPACE, sampling perfection with application optimized contrasts using different flip angle evolutions; TSE, turbo spin echo; VIBE, volumetric interpolated breath-hold examination.

MR attenuation correction

MRAC was based on three-dimensional (3D) Dixon VIBE sequence using the *controlled aliasing in parallel imaging results in higher acceleration* (CAIPIRINHA) technique acquired in transaxial orientation and reconstructed in coronal orientation (Table 1). A coronal μmap was created by segmenting the image data into four compartments with fixed attenuation coefficients: air (0 cm⁻¹), lung (0.0224 cm⁻¹), fat (0.0857 cm⁻¹) and soft tissue (0.1 cm⁻¹). Bone attenuation coefficient was similar to that of a soft tissue. The five-compartment segmentation model was based on the method described by Paulus *et al.* (13). Briefly, μmap images are produced with the four-compartment model, then bone information is added using a model-based bone segmentation algorithm that assigns continuous attenuation coefficients for bones, ranging from 0.1 to 0.2485 cm⁻¹. Only major bones (skull, spine, pelvis and proximal femurs) are included in this model.

PET/CT protocol

Following the PET/MR imaging study, and 60 minutes after the ⁶⁸Ga-PSMA-11 injection, PET/CT imaging was performed on an integrated PET/CT scanner (GEMINI TF, Philips Medical Systems, Cleveland, OH). Prior to the PET/CT study, intravenous iodine contrast media 1.5 cm³/kg (Omnipaque 300; iohexol 0.623 g/mL,

GE Healthcare, Chicago, IL, USA) was administered to all patients except to those with a known iodine hypersensitivity or renal insufficiency. Contrast-enhanced 64-slice multidetector computed tomography (MDCT) was performed from the skull base to the mid-thigh with tube voltage of 120 kVp, spiral CT at 0.8 sec per rotation with modulated 30–250 mAs, section thickness of 3.0 and 3.0 mm intervals with image reconstruction every 3.0 mm. PET emission images were obtained using a weight-based protocol, 2 minutes of acquisition per bed position, with five to six bed positions from the skull base to the mid-thigh. PET data was reconstructed using 3D-OSEM (3 iterations and 20 subsets) on a 144 matrix with CT-based AC.

Image analysis

Image registration between PET and MRI and between PET and CT was validated in our commercial systems.

For each patient, two sets of coronal pelvic μmap images were derived comprising the four and five-compartment segmentation MRAC model (Figure 1).

For each MRAC model, maximal SUVs (SUVmax) were calculated for lesions in the prostate gland, involved lymph nodes and bone metastases. Average SUVs (SUVmean) were calculated in normal appearing tissues, including the prostate gland, gluteus muscle and the sacrum.

Prostate gland lesions were defined as areas with focally increased ⁶⁸Ga-PSMA-11 uptake compared to the contralateral side at the same level and to the adjacent normal-appearing prostate gland. A lymph node was defined as ‘involved’ if it demonstrated increased ⁶⁸Ga-PSMA-11 uptake compared to a contralateral lymph node in a similar lymph node station. Bone metastases were defined as areas with focally increased ⁶⁸Ga-PSMA-11 uptake compared to an adjacent normal-appearing bone. Measurements of prostate lesions, lymph nodes and bone lesions were performed only on one dominant lesion (defined as the most avid lesion) in each site. The four-compartment MRAC image served as reference. For each lesion, the maximal region of interest (ROI) was placed in the four-compartment MRAC image and the SUVmax was measured. SUVmax of the five-compartment MRAC and of the CTAC were determined by copying the ROI from the reference image and applying it onto the respective images.

The SUVmean of the normal sacrum at S1 level and the gluteus were measured. For sacral measurements, a fixed ROI with a diameter of 2 cm was applied. For gluteal measurements a fixed ROI with a diameter of 2.5 cm was placed on the right and left gluteus maximus muscle and

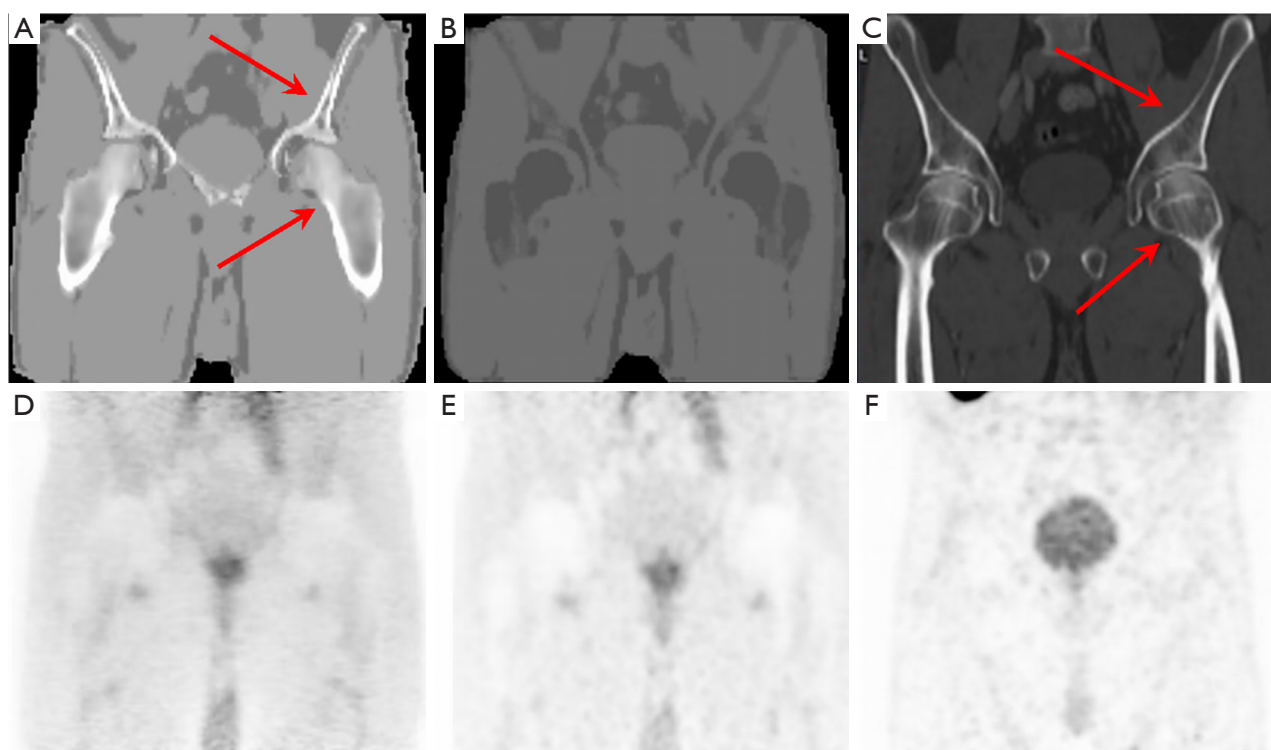


Figure 1 Coronal μ map images of the pelvis of a 63-year-old man with prostate cancer, derived from (A) five and (B) four compartment segmentation model with corresponding MRAC (D,E). A coronal plane CT image of the same area with corresponding CTAC (C,F). These images of the pelvis demonstrate the effect of adding the iliac bones and the femurs (arrows) on AC images. MRAC, magnetic resonance attenuation correction; CTAC, computed tomography attenuation correction.

the average of both measurements was calculated. For the lesional measurements, the four-compartment MRAC images were used as the reference from which the ROI was copied and placed onto the five-compartment MRAC and CTAC images to measure the SUVmean. ‘Lesions’ comprised prostate lesions, lymph nodes and bone metastases. The sum of all lesional SUVmax means was calculated and the lesions to gluteus (L/G) ratio were evaluated.

PET measurements were normalized for body weight and assessed quantitatively using dedicated software (Syngo.via; Siemens AG, Healthcare Sector, Erlangen, Germany).

Studies were interpreted by a consensus read of a board-certified nuclear medicine physician with 12 and 4 years of experience in PET/CT and PET/MR, respectively, and by a radiologist with 8 and 5 years of experience in PET/CT and PET/MR, respectively.

Statistical analysis

The means of SUVmax and SUVmean of the two MRAC

models were compared using paired *t*-test.

The effect size (ES), which shows the magnitude of the difference between the two MRAC models for each tissue, was calculated by Cohen’s *d* statistic:

$$d = \frac{M1 - M2}{S_{pooled}} \quad [1]$$

Where, *d* is the ES, M1 is the mean of the 5-compartment MRAC model, M2 is the mean of the 4-compartment MRAC model and S_{pooled} is the pooled standard deviation for M1 and M2.

ES was defined as very small (<0.2), small (0.21–0.5), medium (0.51–0.8), large (0.81–1.2) and very large (>1.2).

The coefficient of determination (R^2) was calculated for each tissue.

The association between the MRAC models and CTAC was evaluated by Pearson’s correlation (*r*) and interpreted as follows: poor correlation ($0.00 \leq r \leq 0.20$), fair correlation ($0.20 < r \leq 0.40$), moderate correlation ($0.40 < r \leq 0.60$), good correlation ($0.60 < r \leq 0.80$), very good correlation ($r > 0.80$).

Table 2 Differences in SUV measurements between four and five-compartment MRAC

Tissue	MRAC5 SUVs [†] , mean (range)	MRAC4 SUVs [†] , mean (range)	P value	Mean difference (SD)	Effect size	R2 (P value)	R (P value)	95% CI
Gluteus maximus	0.69 (0.43–1.35)	0.77 (0.31–1.62)	0.001	0.08 (0.11)	0.72	0.76 (0.001)	0.87 (<0.0001)	0.79–0.93
Sacrum	1.26 (0.75–1.9)	1.43 (0.78–2.43)	0.013	0.17 (0.31)	0.54	0.56 (0.001)	0.75 (<0.0001)	0.52–0.88
Normal prostatic tissue	2.79 (1.59–24.2)	3.02 (1.7–21.0)	0.003	0.23 (–0.32)	0.72	0.83 (0.001)	0.92 (<0.0001)	0.79–0.97
Intra prostatic cancer	6.83 (2.4–24.2)	7.65 (3.2–21.0)	0.005	0.82 (1.20)	0.68	0.95 (0.001)	0.98 (<0.0001)	0.95–0.99
Metastatic lesions	6.4600 (1.7–17.8)	4.79 (1.59–8.43)	0.173	–1.67	0.54	0.74	0.77 (0.0268)	0.13–0.96
Lesion to gluteus ratio	9.36 (1.96–36.8)	10.15 (2.42–27.8)	0.24	0.79 (3.61)	0.22	0.79 (0.001)	0.95 (<0.0001)	0.90–0.98

[†], for each MRAC model, maximal SUVs (SUVmax) were calculated for lesions in the prostate gland, involved lymph nodes and bone metastases. Average SUVs (SUVmean) were calculated in normal appearing tissues, including the prostate gland, gluteus muscle and the sacrum. SUV, standardized uptake value; MRAC, magnetic resonance attenuation correction; R2, Coefficient of determination of Pearson's correlation; SD, standard deviation; r, Pearson's correlation; R2, coefficient of determination.

Comparison of correlation coefficients was performed using the Z test.

Statistical analysis was carried out using SPSS 22.0 software (SPSS, Chicago, IL, USA) and the MedCalc 16.8 software (MedCalc Software, Ostend, Belgium). Statistical significance was defined as P value <0.05.

Results

Twenty-six patients (mean age, 69.4±9.3 years) were included in the study and underwent ⁶⁸Ga-PSMA-11 PET/CT and ⁶⁸Ga-PSMA-11 PET/MR of the pelvis. Of these, 25 patients presented for staging of prostate cancer and one patient had a prior radical prostatectomy and was evaluated for recurrent disease. Twenty-two prostate lesions were evaluated (one patient had a prior prostatectomy and three patients had no ⁶⁸Ga-PSMA-11 uptake in the prostate gland). Five involved lymph nodes and three bone metastases from different patients were analysed collectively due to their small number. In addition, normal prostate SUVs were measured in 21 patients (of the remaining 5 patients, one had prior prostatectomy and 4 patients had diffuse involvement of the prostate gland). Sacral and gluteal SUVs were measured in all of the patients.

Correlation between four- and five-compartment MRAC models

There was a statistically significant difference between SUVs of the gluteus, sacrum, prostatic lesions and normal prostate tissue measured by the four-compartment *vs.* the five-compartment MRAC models (P=0.001, 0.013, 0.003

and 0.005, respectively; *Table 2*). No statistically significant difference was noted for SUVs of metastases and L/G ratio. The ES for the difference between the models was small for L/G ratio and medium for all other tissues that were measured.

As shown in *Table 2*, SUVs of prostatic lesions, L/G ratio, gluteus and normal prostate gland tissues showed very good correlation (r=0.98, 0.95, 0.87 and 0.92, respectively) between four- and five-compartment MRAC SUVs. SUVs of metastases and sacrum tissue showed good correlation (r=0.77 and 0.75, respectively) between the two MRAC models.

Correlation between four- and five-compartment MRAC models and CTAC model

As shown in *Table 3*, four-compartment MRAC showed very good correlation with CTAC for SUVs of prostatic lesions (r=0.90) and good correlation with CTAC for SUVs of L/G ratio (r=0.74). Five-compartment MRAC showed very good correlation with CTAC for SUVs of prostatic lesions and L/G ratio (r=0.95 and 0.89, respectively), and good correlation with CTAC for SUVs of metastatic lesions (r=0.77). The correlation coefficients between 4-compartment MRAC and CTAC, and between 5-compartment MRAC and CTAC were not clinically significant (*Table 3*).

Discussion

At present, μ map images in PET/MR are commonly attained by using fast volumetric Dixon-based sequences with fat/water separation, yielding four compartments with

Table 3 Correlation between five- and four-compartment MRAC SUV and CTAC SUV

Site	Pearson's correlation (r)			Comparison of correlation coefficients	
	MRAC model	MRAC model SUV vs. CTAC SUV	P value	Z-statistics	P value
Gluteus maximus	MRAC 4	0.231	0.099	0.099	0.92
	MRAC 5	0.250	0.074		
Sacrum	MRAC 4	-0.109	0.596	0.22	0.82
	MRAC 5	-0.174	0.396		
Normal prostatic tissue	MRAC 4	0.473	0.031	0.15	0.87
	MRAC 5	0.514	0.017		
Intra prostatic cancer	MRAC 4	0.896	0.001	0.97	0.32
	MRAC 5	0.947	0.001		
Metastatic lesions	MRAC 4	0.369	0.368	0.97	0.32
	MRAC 5	0.766	0.027		
Lesion/gluteus ratio	MRAC 4	0.739	0.001	0.68	0.31
	MRAC 5	0.892	0.001		

CTAC, computed tomography attenuation coefficient; MRAC, magnetic resonance attenuation coefficient; SUV, standardized uptake value.

fixed attenuation coefficients (air, lung, fat and soft tissue). MRAC of bones has been a technical challenge because the MR signal of cortical bones is very low, resembling the AC of air, and dedicated sequences for bone imaging using ultrashort or zero time to echo (UTE and ZTE, respectively) are time consuming. As a result, dedicated bone sequences have been applied in limited cases, such as head imaging. In other cases, such as whole-body imaging, attenuation coefficient of soft tissues was assigned to bones. Several studies have evaluated the effect of soft tissue to bone AC substitution on PET quantification and reported differences of approximately 10% in tracer uptake in soft tissue lesions and bone lesions (2). Keereman *et al.* have shown a difference of 2–17.5% in tracer uptake when cortical bone AC was replaced with soft tissue AC in a simulated phantom model. In that study the relative error for uptake in the prostate gland was 4.2% (14). Samarin *et al.* examined the impact of replacing bone AC with soft tissue AC in PET/CT and reported an underestimation range of 1.5–30.8% for uptake in bone lesions and of 0.2–4% for uptake in lesions located adjacent to bone (15). All of these studies have emphasized the importance of adding a bone compartment for accurate PET quantification.

Our PET/MR software uses a model-based AC method for bone segmentation. Paulus *et al.* reported that SUV

underestimation in bone lesions decreased from 7.3% to 2.9% using this model (13). Oehmigen *et al.* (3) evaluated the impact of applying a five-compartment segmentation model with bone segmentation over the four-compartment model. Quantification of SUVmax in 99 lesions showed that the highest increase in SUVmax was in bone lesions with an average of $1.4\% \pm 2.5\%$ (3).

In contrast to previously mentioned studies, which used ^{18}F -FDG as a radiotracer, Elschot *et al.* have investigated the effect of adding bone segmentation to PET quantification in prostate cancer patients who underwent PET/MR with ^{18}F -fluciclovine, a dedicated prostate cancer radiotracer. They found that the differences in SUVmax in the prostate bed and in lymph node lesions were 2–3%, and concluded that inclusion of bone segmentation is of no value for clinical evaluation of soft tissue lesions (4).

To the best of our knowledge, the current study is the first to evaluate the effect of incorporation of bone segmentation on PET quantification using ^{68}Ga -PSMA-11. We found significant differences in SUV between the four-compartment and the five-compartment model (which includes bone segmentation), with an average difference of 12% for prostatic lesions and 8% for normal prostatic tissue. These differences are more prominent than those reported in other studies. This might be attributed to the

higher specificity of ⁶⁸Ga-PSMA-11, compared to FDG, in prostate lesions, which resulted in higher SUVs and therefore in a more prominent effect on AC. The normal sacrum also demonstrated significant difference in uptake between the four-compartment model and the five-compartment model, whereas the lack of difference between the two models in uptake in metastases might be attributed to the small number of lesions that were assessed and to the summation of SUVs from bone lesions and involved lymph nodes. As PET quantification is very important for characterizing lesions and for evaluating the response to therapy on sequential studies, our results suggest that follow-up studies must be performed with the same body segmentation.

Our study has several limitations. First, the small number of patients limits its power. Second, the study's retrospective nature has inherent limitations. Third, the small number of lesions, particularly the small number of metastases precludes reaching a definitive conclusion, which is reflected in the relatively low ES. Fourth, although very good to good correlation was found between MRAC and CTAC for prostatic lesions, SUVmax was not compared among the models due to the different time interval between radiotracer injection and scanning of the patient; therefore no definite conclusion can be drawn regarding the superiority of one model compared to the other.

In conclusion, our preliminary findings indicate, for the first time, that the addition of bone segmentation to the commonly-used four-compartment segmentation model has an impact on SUV measurements both in prostate lesions and in the normal prostate, indicating that patient follow-up studies must be conducted using the same segmentation model. Larger studies are warranted to validate the use of the five-compartment segmentation model which includes bone segmentation in prostate cancer patients undergoing ⁶⁸Ga-PSMA-11 PET/MR.

Acknowledgments

The authors acknowledge Zohar Nitsan, Inbal Machcat, and Hagai Baruch for their excellent work in patient scanning, Dr. Limor Shaharabani-Gargir for patient management and Dr. Sharon Furman-Assaf for editing.

Footnote

Conflicts of Interest: The authors have no conflicts of interest to declare.

Ethical Statement: This study was approved by the institutional ethics committee (approval number, 2015024). Written informed consent was obtained from all patients prior to study participation.

References

1. Martinez-Moller A, Souvatzoglou M, Delso G, Bundschuh RA, Chefd'hotel C, Ziegler SI, Navab N, Schwaiger M, Nekolla SG. Tissue classification as a potential approach for attenuation correction in whole-body PET/MRI: evaluation with PET/CT data. *J Nucl Med* 2009;50:520-6.
2. Aznar MC, Sersar R, Saabye J, Ladefoged CN, Andersen FL, Rasmussen JH, Lofgren J, Beyer T. Whole-body PET/MRI: the effect of bone attenuation during MR-based attenuation correction in oncology imaging. *Eur J Radiol* 2014;83:1177-83.
3. Oehmigen M, Lindemann ME, Gratz M, Kirchner J, Ruhlmann V, Umutlu L, Blumhagen JO, Fenchel M, Quick HH. Impact of improved attenuation correction featuring a bone atlas and truncation correction on PET quantification in whole-body PET/MR. *Eur J Nucl Med Mol Imaging* 2018;45:642-53.
4. Elschot M, Selnaes KM, Johansen H, Kruger-Stokke B, Bertilsson H, Bathen TF. The Effect of Including Bone in Dixon-Based Attenuation Correction for (18) F-Fluciclovine PET/MRI of Prostate Cancer. *J Nucl Med* 2018;59:1913-7.
5. Park SY, Zacharias C, Harrison C, Fan RE, Kunder C, Hatami N, Giesel F, Ghanouni P, Daniel B, Loening AM, Sonn GA, Iagaru A. Gallium 68 PSMA-11 PET/MR Imaging in Patients with Intermediate- or High-Risk Prostate Cancer. *Radiology* 2018;288:495-505.
6. Eiber M, Weirich G, Holzapfel K, Souvatzoglou M, Haller B, Rauscher I, Beer AJ, Wester HJ, Gschwend J, Schwaiger M, Maurer T. Simultaneous ⁶⁸Ga-PSMA HBED-CC PET/MRI Improves the Localization of Primary Prostate Cancer. *Eur Urol* 2016;70:829-36.
7. Al-Bayati M, Grueneisen J, Lutje S, Sawicki LM, Suntharalingam S, Tschirdewahn S, Forsting M, Rubben H, Herrmann K, Umutlu L, Wetter A. Integrated ⁶⁸Gallium Labelled Prostate-Specific Membrane Antigen-11 Positron Emission Tomography/Magnetic Resonance Imaging Enhances Discriminatory Power of Multi-Parametric Prostate Magnetic Resonance Imaging. *Urol Int* 2018;100:164-71.
8. Domachevsky L, Goldberg N, Bernstine H, Nidam M, Groshar D. Quantitative characterisation of clinically

- significant intra-prostatic cancer by prostate-specific membrane antigen (PSMA) expression and cell density on PSMA-11. *Eur Radiol* 2018;28:5275-5283:5275-83.
9. Domachevsky L, Bernstine H, Goldberg N, Nidam M, Stern D, Sosna J, Groshar D. Early (68)Ga-PSMA PET/MRI acquisition: assessment of lesion detectability and PET metrics in patients with prostate cancer undergoing same-day late PET/CT. *Clin Radiol* 2017;72:944-50.
 10. Freitag MT, Radtke JP, Hadaschik BA, Kopp-Schneider A, Eder M, Kopka K, Haberkorn U, Roethke M, Schlemmer HP, Afshar-Oromieh A. Comparison of hybrid (68)Ga-PSMA PET/MRI and (68)Ga-PSMA PET/CT in the evaluation of lymph node and bone metastases of prostate cancer. *Eur J Nucl Med Mol Imaging* 2016;43:70-83.
 11. Thalgott M, Duwel C, Rauscher I, Heck MM, Haller B, Gafita A, Gschwend JE, Schwaiger M, Maurer T, Eiber M. One-stop shop whole-body (68)Ga-PSMA-11 PET/MRI compared to clinical Nomograms for preoperative T- and N-Staging of High-Risk Prostate Cancer. *J Nucl Med* 2018;59:1850-6.
 12. Domachevsky L, Bernstine H, Goldberg N, Nidam M, Catalano OA, Groshar D. Comparison between pelvic PSMA-PET/MR and whole-body PSMA-PET/CT for the initial evaluation of prostate cancer: a proof of concept study. *Eur Radiol* 2020;30:328-36.
 13. Paulus DH, Quick HH, Geppert C, Fenchel M, Zhan Y, Hermosillo G, Faul D, Boada F, Friedman KP, Koesters T. Whole-Body PET/MR Imaging: Quantitative Evaluation of a Novel Model-Based MR Attenuation Correction Method Including Bone. *J Nucl Med* 2015;56:1061-6.
 14. Keereman V, Holen RV, Mollet P, Vandenberghe S. The effect of errors in segmented attenuation maps on PET quantification. *Med Phys* 2011;38:6010-9.
 15. Samarin A, Burger C, Wollenweber SD, Crook DW, Burger IA, Schmid DT, von Schulthess GK, Kuhn FP. PET/MR imaging of bone lesions--implications for PET quantification from imperfect attenuation correction. *Eur J Nucl Med Mol Imaging* 2012;39:1154-60.

Cite this article as: Domachevsky L, Goldberg N, Gorenberg M, Bernstine H, Groshar D, Catalano OA. Prostate cancer evaluation using PET quantification in ⁶⁸Ga-PSMA-11 PET/MR with attenuation correction of bones as a fifth compartment. *Quant Imaging Med Surg* 2020;10(1):40-47. doi: 10.21037/qims.2019.11.19